



Two distinct branch–stem interfacial structures of silver dendrites with vertical and slanted branchings

Shaochun Tang, Sascha Vongehr, Xiangkang Meng*

National Laboratory of Solid State Microstructures, Department of Materials Science and Engineering, Nanjing University, Nanjing 210093, People's Republic of China

ARTICLE INFO

Article history:

Received 12 May 2009

In final form 26 June 2009

Available online 1 July 2009

ABSTRACT

Silver dendrites synthesized by sonoelectrochemical deposition are investigated via transmission electron microscopy (TEM) in order to clarify the formation of specific branching angles. Two kinds of dendrites are found to form simultaneously; one has slanted angles while the other shows orthogonal branching. Investigation of the branch–stem interfacial structures reveals that the vertical branches attach at a characteristic transition layer around the main stem, while the slanted growth involves twinning induced dislocations. It is suggested that oriented attachment of nanoparticles followed by epitaxial growth leads to obliqueness, while crystallization of amorphous phase involving grain rotation and realignment results in vertical branching.

© 2009 Elsevier B.V. All rights reserved.

1. Introduction

Much effort has been devoted to understand non-equilibrium growth phenomena theoretically and experimentally [1,2]. Among such phenomena, dendrites are one of the most intensively investigated topics due to their attractive structures and large surface area [3], both leading to many applications, for example in catalysis [4], chemical/biochemical sensors [5] and surface-enhanced Raman scattering [6]. Detailed description of the structure is important to understand the underlying growth mechanisms, which in turn is crucial to achieve designable structures (e.g. with well defined branch–stem angles) resulting in desired properties. Many studies have focused on the mechanisms of dendritic growth [1,2,7–10]. Some novel growth scenarios have been recently proposed. Ding et al. [9] reported a double-interface growth mode of silver in a replacement reaction where dendritic growth was controlled by the formation of an amorphous phase and its crystallization. Cheng et al. [8] demonstrated that dendritic structure can emerge from oriented attachment of nanoparticles. Ostwald ripening forms the initial particles and also smoothes the morphology after attachment. Dislocations are known to originate at the bonding interface in the oriented attachment of nanoparticles [7,8].

As for growth under non-equilibrium conditions, the distance from equilibrium is important [11,12] but generally not easily controlled [13]. Electrochemistry is in this context especially convenient, because the ‘distance’ can be tuned continuously and reversibly by the electrode potential. Particular attention has been focused on the study of the formation and growth of silver

dendrites by various sonoelectrochemical methods with the assistance of organic capping agents such as nitrilotriacetate [14], gelatin [15] and poly (vinyl pyrrolidone) [16]. Generally, branching angles vary in a range from 15° to 90° [5]. Many factors affecting structure have been discussed [2,13,16], but the detailed growth mechanisms are still unknown. It remains unclear how the branches emerge from the stems; how the interplay of nucleation and growth at the microscopic scale results in specific densities, branching angles and so on.

In this work, we describe the discovery and investigation of two branch–stem interfacial structures occurring simultaneously in a sonoelectrochemical process involving silver: the surfactant-free, constant-current method leads to both, vertical branching and also a slanted growth, sometimes even along the same stem. High resolution transmission electron microscopy (HRTEM) reveals two distinct microstructures underlying the different interfaces. The origin of such dissimilar interfacial structures will be discussed in light of the many new proposals concerning non-equilibrium growth.

2. Experiment

Silver dendrites were fabricated by a sonoelectrochemical reaction with silver perchlorate solutions as electrolytes. The simple two-electrode setup was described previously [16–19]. Two identical silver sheets (2 cm × 2 cm) were cleaned with acetone, hydrochloric acid and distilled water to remove surface contamination. The sheets were fixed on the two opposing sides of an electrochemical cell 4 cm apart in order to serve as the working cathode and counter anode. The electrolyte concentration (C), current density (J), and the reaction time (t) were about 1.0×10^{-4} to 5×10^{-3}

* Corresponding author. Fax: +86 25 8359 5535.

E-mail address: mengxk@nju.edu.cn (X. Meng).

mol/L, 1.25 to 2.5 mA/cm² and 10 to 20 min, respectively. Electrolysis was conducted at room temperature under continuous 40 kHz ultrasonic vibration at 50 W power. Products were precipitated and purified by five centrifugation/rinsing/redispersion steps with deionized water and ethanol.

The products were collected, dried at 40 °C for 12 h in an oven, and characterized by X-ray diffraction (XRD) with a D/Max-RA X-ray diffractometer (using Cu K α = 1.5418 Å radiation). Transmission electron microscopy (TEM) samples were prepared by dripping suspensions of the dendrites onto a carbon film covering a copper grid and subsequent drying. TEM measurement was performed with an FEI TECNAI F20 microscope operating at 200 kV.

3. Results and discussion

Fig. 1 shows an XRD pattern of the as-synthesized product from a typical experiment (C, V and t were 1.1×10^{-3} mol/L, 1.25 mA/cm² and 20 min). The XRD pattern reveals that these Ag dendrites are cubic Ag ($a = 4.09$ Å, JCPDS 04-0783). The diffraction peaks observed can be indexed as (1 1 1), (2 0 0), (2 2 0) and (3 1 1) planes of the face-centered cubic (fcc) structure, respectively. An absence of other peaks indicates a high purity of the silver.

Over the whole range of investigated conditions, the sonoelectrochemical reaction always produces two types of dendrites. In the TEM images they are easily distinguished by their specific angles between branches and the main stem. TEM images of two typical dendritic structures in the product (Fig. 1) are shown in Fig. 2a and b. In Fig. 2a, the branches are approximately parallel to each other and attach basically perpendicular to the stem (branching angle is 90°). Also, most branches point towards one side of the stem. The structure looks two dimensional although it grew in solution. It is known that the growth happened in solution, because without ultrasound irradiation, all the products adhere to the cathode while the electrolyte remains clear, and our TEM observations (not shown) evidenced that the products adhering to the cathode are large conglomerates totally different from the dendrites shown in Fig. 2a. The branches of the dendrite in Fig. 2b show angles of 53–61° towards the main stem; coinciding with many previous reports [5,20,21]. Such angles indicate that the growth is globally diffusion-controlled. This slanted branching is more commonly observed under non-equilibrium conditions [5,16,21,22] and also happens to be the more prominent in our products. The insets in Fig. 2a and b magnify the areas inside the white dashed squares

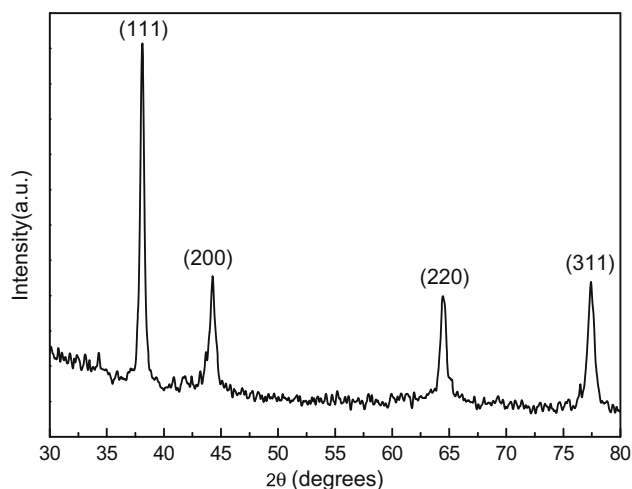


Fig. 1. XRD pattern of as-synthesized silver dendrites.

and exhibit the branching angles more clearly, i.e. a vertical (inset of Fig. 2a) and a slanted growth (inset of Fig. 2b) clearly distinguishes the dendrites. Sometimes, both types of growth even appear on different sections of the same individual dendrite (Fig. 2c). The areas representing vertical and slanted growth are denoted as area 'V' and 'S', respectively.

To reveal the origin of such dissimilar branchings, the branch-stem interfacial structure was analyzed with much higher resolution. Fig. 3a shows a magnification of the area V, and the inset further magnifies the squared area (black dashed). The strong contrast between the innermost and subsequent outer parts of the stem in area V suggests a core-shell structure. We henceforth call this subsequent shell 'transition layer', because there is yet another outermost coating. That outermost surface of the dendrite is less obvious (has less contrast) and is therefore specifically labeled in the inset of Fig. 3a. A HRTEM image (Fig. 3b) magnifying the area inside the larger dashed square in the inset of Fig. 3a reveals that the outermost layer is amorphous, which indicates that an amorphous phase or growth front may have been forming first in this sonoelectrochemical growth process. A few very small crystallites with different crystallographic orientations are present in the amorphous layer (arrows in the inset of Fig. 3a and white dashed circles in 3b). Such an amorphous layer has been observed in the growth of silver dendrites fabricated by a replacement reaction [9]. Similar amorphous regions involving InAs dendrites were reported by May et al. [23]. It is clearly seen (Fig. 3b) that the transition layer is single-crystalline. The fringe spacing of 0.23 nm implies that these are interplanar spacings of (1 1 1) planes. Moreover, these fringes run continuously through both the transition layer and the branch. Both belong to a single crystal and the connection between branch and stem is not simply a physical contact but rather like an epitaxial growth. The branches are *not* perpendicular to the stem without the presence of the transition layer, as shown in the upper section of the dendrite in Fig. 2c. The vertical growth of branches is therefore attributed to this transition layer. The core-shell interface between the transition layer and the inner dark region (labeled 'interface 2' in Fig. 3b) is further investigated with the images 3c and 3d. Fig. 3c shows the fast Fourier transforms (FFT) of the areas A, B and C. The similarity between all the hexagonal FFT patterns indicates that the transition layer and the inner stem all belong to fcc silver. The electron beam transmits through the whole core-shell structure, and the two types of spots in the FFT corresponding to areas B and C demonstrate the core-shell structure of stem and surrounding transition layer. Fig. 3d displays the HRTEM of the smaller dashed square in the inset of Fig. 3a. From the FFT pattern one can determine that the direction orthogonal to $\langle 1\ 1\ -1 \rangle$ in Fig. 3d is $\langle 0\ 1\ 1 \rangle$. Also the branching direction is indicated in Fig. 3d, and it is parallel to the arrow in the inset of Fig. 3a; there is no rotation between the images at different magnifications. The branching direction happens to lie at about 30° away from $\langle 0\ 1\ 1 \rangle$, i.e. it is not related to any specific crystallographic direction (e.g. a well known fast direction or suchlike). This implies that the branching angle is under the control of global diffusion while the crystal directions had an influence only locally (grain rotation and realignment).

The slanted branching from the circled area 'S' of Fig. 2c, is further investigated with Fig. 4. It can be seen that the branches have round cross sections (Fig. 4a). The dendrite has a bilaterally symmetric structure with branches distributed roughly evenly between the sides of the stem. Fig. 4b magnifies the squared area in Fig. 4a; no transition layer is visible. The HRTEM image in Fig. 4b shows a connection between a stem and one of the branches (the square in Fig. 4a). It shows edge dislocations at the connecting region between the crystal structure of the stem and that of the branch (twinning), which both turn out to be single-crystalline domains. The fringe spacings perpendicular to twin plane are

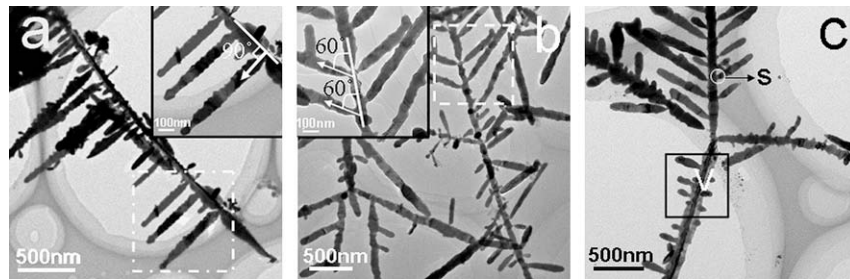


Fig. 2. TEM images of typical silver dendrites (a) the vertical growth and (b) the slanted branching. The insets in the corners are magnifications of the dashed squares and (c) an individual silver dendrite including both kinds of branchings.

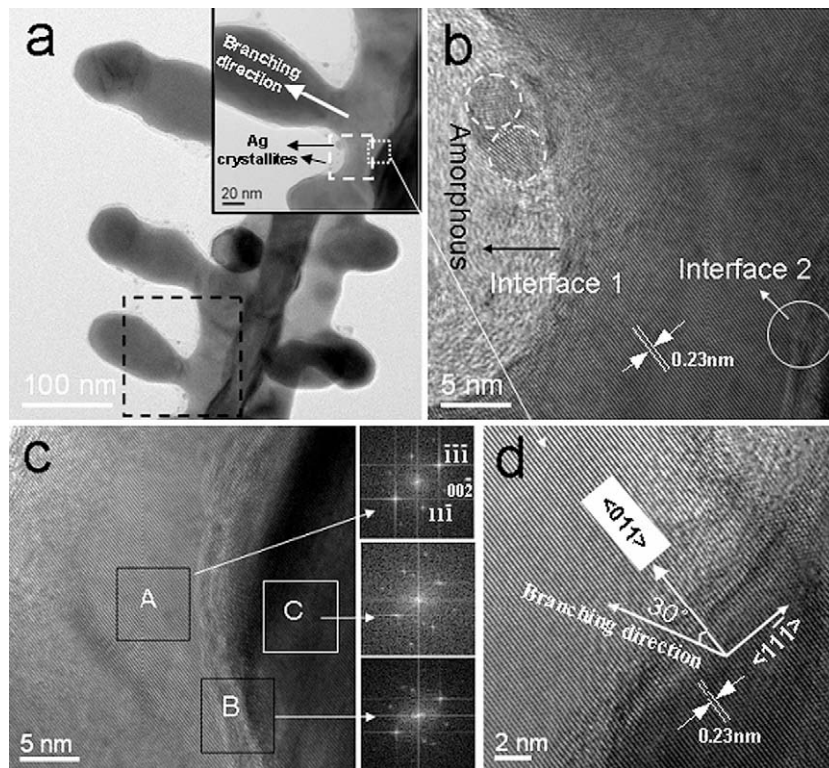


Fig. 3. TEM and HRTEM images of a typical silver dendrite (a) local-magnification of area V in Fig. 2c; the inset further magnifies the black dashed square, (b) HRTEM image magnifying the area inside the larger dashed square in the inset of (3a), (c) HRTEM image of the area of 'interface 2' indicated in image (b). The right-hand insets are the FFT patterns corresponding to the squared areas labeled A, B, and C, and (d) HRTEM with even higher resolution showing the smaller dashed square in the inset of (3a).

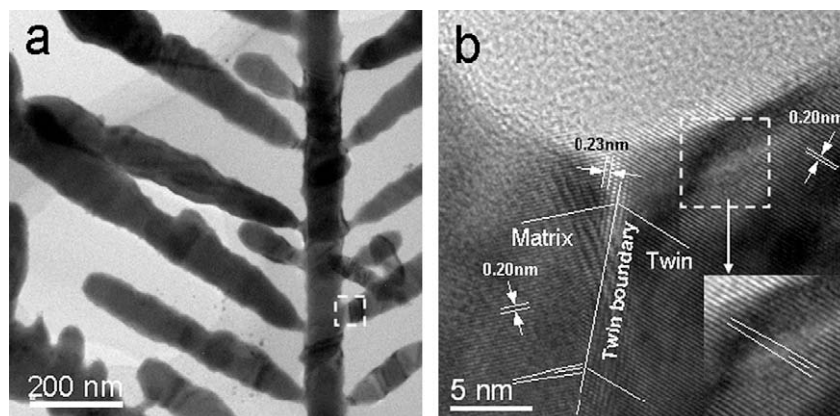


Fig. 4. (a) The area S shown in Fig. 2c, and (b) HRTEM image of the squared area in (a).

measured to be 0.23 nm, which indicates (1 1 1) interplanar spacing. Another set of fringes in the branch displays the (1 0 0) interplanar spacing of 0.20 nm, but the thereby inferred $\langle 100 \rangle$ direction is not quite parallel to the branch. This is expected, because the branching angles are 53–61°, so they are not exactly equal but quite close to the angle of 54.7° between the $\langle 100 \rangle$ and the $\langle 111 \rangle$ direction perpendicular to the (1 1 1) twin plane (Fig. 4b). Such angles indicate that the growth is globally diffusion-controlled, but locally it results from oriented attachment, which has been found to be responsible for the formation dislocations during early crystal growth [24]. Nano-particle aggregation by oriented attachment of nano-crystallites, has been recognized as an important crystal growth mechanism for dendritic morphology in solution [7,8,25–28]. The formation of dislocations is often a direct consequence of oriented attachment of a nano-particle that attaches with a small misorientation or atomic nonflatness at the bonding interface, and so marks the occurrence of the initial particle–particle bonding [8,24] that initiates a new branch. The inset again magnifies the marked square just above in order to point out another edge dislocation (defined as having a Burgers vector normal to the dislocation line) found within the connecting region. Dislocations formed at interfaces due to oriented attachments in other systems have also been reported by Penn and Banfield [8,24]. The formation of defects coincides with the direct (no transition layer), slanted branching.

Our TEM observations reveal that two types of branch–stem interfacial structures can appear even on the same silver dendrite. This results from different nucleation and growth modes of the branches on the stem. Generally, branch formation involves several growth mechanisms: atom-by-atom crystal growth, amorphous growth with later crystallization, oriented attachment of nanoparticles and grain rotation and realignment, etc. Also in the case of our sonoelectrochemical deposition system one can expect that some of these mechanisms are responsible for the specific dendrite branching angles. The proposed growth mechanisms for the here observed silver dendrites are as follows:

- (1) In the slanted growth, the attachment of a nanoparticle seed to the stem's surface forms a nucleus for the growth of a side branch. The observed twins and twinning induced dislocations (Fig. 4b) are indicative of this. Regularities in dendrite side branches (frequency and angle) can be attributed to twinning [29]. Twinning is a common result of two fcc structures joining with their {1 1 1} facets to share a crystallographic plane [30]. Such oriented attachment has been found to be responsible for the dislocations during early crystal growth [24]. In the slanted growth mode observed here, the branching angles are not exactly 55°, and therefore they are likely affected by the diffusion of Ag precursors [5]. The epitaxial crystal growth via atom-by-atom addition develops a single-crystalline branch.
- (2) As for the vertical growth, this orthogonality is well known to arise from growth within an amorphous layer, as observed during vapor deposition experiments using catalyst [23]. Indeed, we found the transition layer around the main stem and a small amorphous layer around the whole structure to be always present in vertically grown dendrites. In our sonoelectrochemical deposition process, silver may first deposit to form an initially amorphous phase (as similarly observed by Ding et al. [9]) departing orthogonally from the stem. In the area behind the growth front, amorphous silver spontaneously crystallizes and matures by grain rotation and realignment. This is also indicated by the presence of very small grains with different orientations. The later observable transition layer is the matured part of this deposition process from amorphous Ag.

A hypothesis consistent with the appearance of both growth modes during the same experiment is a strong influence of the ultrasound. Compared to the micro scale, ultrasound has a long wavelength and is thus always focused differently at different locations in the reaction vessel (standing wave patterns). Thus, it provides different growth environments resulting in different growth modes during the same experiment. Ultrasonic vibration may play an important role especially for the vertical growth of the branches because it is very difficult to find vertical branches for electrochemically grown silver dendrites without ultrasonic vibration [31]. Such strong influence on the growth mechanism has been suggested previously for the case of Ag sonoelectrochemical deposition on silica spheres from AgNO₃ solution [32].

4. Conclusion

In summary, our study shows an interesting phenomenon in sonoelectrochemical growth processes where two branching angles are found to coincide with distinct branch–stem interfacial micro structures. It is proposed that during slanted branching, the attachment of nanoparticle seeds to the stem's surface results in the observed twinning and its characteristic small edge dislocations. The epitaxial crystal growth via atom-by-atom addition develops a single-crystalline branch. During the vertical growth of branches, silver may first deposit to form an initially amorphous phase (growth front) departing orthogonally from the stem. Silver nucleation in the amorphous layer matures the growing branch via grain rotations into a single crystal. This work advances the understanding of the underlying growth mechanisms in dendrite branching, which may be useful to achieve designable structures (e.g. with well defined branch–stem angles) resulting in desired properties.

Acknowledgments

This work was supported by a grant from the State Key Program for Basic Research of China (2004CB619305), and National Natural Science Foundation of China (50571044 and 50831004).

References

- [1] E. Ben-Jacob, P. Garik, *Nature* 343 (1990) 523.
- [2] V. Fleury, *Nature* 390 (1997) 145.
- [3] Md.H. Rashid, T.K. Mandal, *J. Phys. Chem. C* 111 (2007) 16750.
- [4] S.T. Selvan, T. Hayakawa, M. Nogami, M. Moller, *J. Phys. Chem. B* 103 (1999) 7441.
- [5] X.G. Wen, Y.T. Xie, M.W.C. Mak, K.Y. Cheung, X.Y. Li, R. Renneberg, S.H. Yang, *Langmuir* 22 (2006) 4836.
- [6] W. Song, Y.C. Cheng, H.Y. Jia, W.Q. Xu, B. Zhao, *J. Colloid Interf. Sci.* 298 (2006) 765.
- [7] L. Lu, A. Kobayashi, Y. Kikkawa, K. Tawa, Y. Ozaki, *J. Phys. Chem. B* 110 (2006) 23234.
- [8] Y. Cheng, Y.S. Wang, D.Q. Chen, F. Bao, *J. Phys. Chem. B* 109 (2005) 794.
- [9] J.X. Fang, X.N. Ma, H.H. Cai, X.P. Song, B.J. Ding, *Appl. Phys. Lett.* 89 (2006) 173104.
- [10] G. González, M. Rosso, E. Chassaing, *Phys. Rev. E* 78 (2008) 011601.
- [11] Y. Oaki, H. Imai, *Cryst. Growth Des.* 3 (2003) 711.
- [12] K. Fukami et al., *J. Phys. Chem. C* 111 (2007) 1150.
- [13] J.J. Hoyt, M. Asta, A. Karma, *Mater. Sci. Eng. R* 41 (2003) 121.
- [14] J. Zhu, S. Liu, O. Palchik, Y. Koltypin, A. Gedanken, *Langmuir* 16 (2000) 6396.
- [15] S.W. Liu, W.P. Huang, S.G. Chen, S. Avivi, A. Gedanken, *J. Non-cryst. Solids* 283 (2001) 231.
- [16] S.C. Tang, X.K. Meng, H.B. Lu, S.P. Zhu, *Mater. Chem. Phys.* 116 (2009) 464.
- [17] S.C. Tang, Y.F. Tang, F. Gao, Z.G. Liu, X.K. Meng, *Nanotechnology* 18 (2007) 295607.
- [18] S.C. Tang, Y.F. Tang, S.P. Zhu, H.M. Lu, X.K. Meng, *J. Solid State Chem.* 180 (2007) 2871.
- [19] S.C. Tang, S.P. Zhu, H.M. Lu, X.K. Meng, *J. Solid. State Chem.* 181 (2008) 587.
- [20] Q. Zhou, S. Wang, N.Q. Jia, L. Liu, J.J. Yang, Z.Y. Jiang, *Mater. Lett.* 60 (2006) 3789.
- [21] Sreejith Kaniyankandy, J. Nuwad, C. Thinaharan, G.K. Dey, C.G.S. Pillai, *Nanotechnology* 18 (2007) 125610.

- [22] J.X. Fang, H.J. You, C. Zhu, P. Kong, M. Shi, X.P. Song, B.J. Ding, *Chem. Phys. Lett.* 439 (2007) 204.
- [23] S.J. May, J.G. Zheng, B.W. Wessels, L.J. Lauhon, *Adv. Mater.* 17 (2005) 598.
- [24] R.L. Penn, J.F. Banfield, *Science* 281 (1998) 969.
- [25] A. Dougherty, P.D. Kaplan, J.P. Gollub, *Phys. Rev. Lett.* 58 (1987) 652.
- [26] R. Pieters, J.S. Langer, *Phys. Rev. Lett.* 56 (1987) 1948.
- [27] D.E. Zhang, X.J. Zhang, X.M. Ni, J.M. Song, H.G. Zheng, *Chem. Phys. Lett.* 430 (2006) 326.
- [28] R. He, X.F. Qian, J. Yin, Z.K. Zhu, *Chem. Phys. Lett.* 369 (2003) 454.
- [29] A.R. Despic, K.I. Popov, Transport controlled deposition and dissolution of metals, modern aspects of electrochemistry, No. 7, in: B.E. Conway, J.O.M. Bockris (Eds.), Plenum Press, New York, 1972 (Chapter 4).
- [30] Z.L. Wang, *J. Phys. Chem. B* 104 (2000) 1153.
- [31] J.X. Fang, H. Hahn, R. Krupke, F. Schramm, T. Scherer, B.J. Ding, X.P. Song, *Chem. Commun.* 1130 (2009).
- [32] V.G. Pol, D.N. Srivastava, O. Palchik, V. Palchik, M.A. Slifkin, A.M. Weiss, *A. Gedanken, Langmuir* 18 (2002) 3352.